Structure and function of the Leptospira interrogans peroxide stress regulator (PerR), an atypical PerR devoid of a structural metal-binding site

Mounira Kebouchi, Frederick Saul, Raleb Taher, Annie Landier, Bénédicte Beaudeau, Sarah Dubrac, Patrick Weber, Ahmed Haouz, Mathieu Picardeau, Nadia Benaroudj

Structure and function of the *Leptospira interrogans* peroxide stress regulator (PerR), an atypical PerR devoid of a structural metal-binding site

Received for publication, June 28, 2017, and in revised form, November 10, 2017 Published, Papers in Press, November 16, 2017, DOI 10.1074/jbc.M117.804443

Mounira Kebouchi[‡1], Frederick Saul[§], Raléb Taher[‡2], Annie Landier[‡], Bénédicte Beaudeau[‡], Sarah Dubrac[¶], Patrick Weber[§], Ahmed Haouz[§], Mathieu Picardeau[‡3], and Nadia Benaroudj[‡4]

From the [‡]Unité de Biologie des Spirochètes, [§]Plate-forme de Cristallographie, CNRS UMR 3528, and [¶]Unité de Biologie des Bactéries Pathogènes à Gram Positif, Institut Pasteur, F-75015 Paris, France

Edited by F. Peter Guengerich

Peroxide sensing is essential for bacterial survival during aerobic metabolism and host infection. Peroxide stress regulators (PerRs) are homodimeric transcriptional repressors with each monomer typically containing both structural and regulatory metal-binding sites. PerR binding to gene promoters is controlled by the presence of iron in the regulatory site, and iron-catalyzed oxidation of PerR by H_2O_2 leads to the dissociation of PerR from DNA. In addition to a regulatory metal, most PerRs require a structural metal for proper dimeric assembly. We present here a structural and functional characterization of the PerR from the pathogenic spirochete *Leptospira interrogans*, a rare example of PerR lacking a structural metal-binding site. *In vivo* studies showed that the leptospiral PerR belongs to the peroxide stimulon in pathogenic species and is involved in controlling resistance to peroxide. Moreover, a *perR* mutant had decreased fitness in other host-related stress conditions, including at 37 °C or in the presence of superoxide anion. *In vitro*, leptospiral PerR could bind to the *perR* promoter region in a metal-dependent manner. The crystal structure of the leptospiral PerR revealed an asymmetric homodimer, with one monomer displaying complete regulatory metal coordination in the characteristic caliper-like DNA-binding conformation and the second monomer exhibiting disrupted regulatory metal coordination in an open non-DNA–binding conformation. This structure showed that leptospiral PerR assembles into a dimer in which a metal-induced conformational switch can occur independently in the two monomers. Our study demonstrates that structural metal binding is not compulsory for PerR dimeric assembly and for regulating peroxide stress.

This work was supported by the Institut Pasteur and Agence National de la Recherche Grant ANR-08-MIE-018. The authors declare that they have no conflicts of interest with the contents of this article.

The atomic coordinates and structure factors (code 5NL9) have been deposited in the Protein Data Bank (http://wwpdb.org/).

This article contains Tables S1 and S2 and Figs. S1–S7.

[1] Present address: Unité de Recherche Animale et Fonctionalité des Produits Animaux, INRA Université de Lorraine UR AFPA-PB2P, 54518 Vandoeuvre-lès-Nancy, France.

[2] Present address: Institut de Biologie Structurale 71 avenue des Martyrs, 38044 Grenoble Cedex 9, France.

[3] To whom correspondence may be addressed. Tel.: 33-1-45-68-83-68; Fax: 33-1-40-61-30-01; E-mail: mathieu.picardeau@pasteur.fr.

[4] To whom correspondence may be addressed. Tel.: 33-1-40-61-37-46; Fax: 33-1-40-61-30-01; E-mail: nadia.benaroudj@pasteur.fr.

Bacteria are unavoidably exposed to reactive oxygen species (ROS)[5] during the course of aerobic metabolism. ROS include superoxide anion radicals ($O_2^{\cdot-}$) and hydrogen peroxide (H_2O_2) produced by the sequential reduction of oxygen catalyzed by membrane-associated respiratory chain enzymes and hydroxyl radicals ($^{\cdot}OH$) subsequently produced from H_2O_2 through the Fenton reaction (1). Environmental agents, such as ionizing UV radiation, also contribute to increase the $O_2^{\cdot-}$ cellular content. Pathogenic bacteria are also exposed to a variety of oxidants, such as $O_2^{\cdot-}$, $^{\cdot}OH$, and H_2O_2 as well as hypochlorous acid (HOCl) and nitric oxide ($^{\cdot}NO$) produced by the host immune system (2). Defenses against these toxic compounds are therefore crucial for bacterial survival inside and outside the host. Among the multiple enzymes dedicated to ROS detoxification, catalase and other peroxidases catalyze the degradation of H_2O_2 to H_2O. The genes encoding peroxidases in bacteria are under the transcriptional control of H_2O_2 sensors, OxyR and peroxide stress regulator (PerR). With few exceptions, OxyR and PerR do not coexist in the same bacterial species but are present in most Gram-negative or Gram-positive bacteria, respectively (3).

PerRs are homodimeric metalloregulators belonging to the ferric uptake regulator (Fur) family, which act mainly as repressors. The paradigm of PerRs is that of *Bacillus subtilis*, which has been well characterized (4). The individual monomers of PerR consist of an N-terminal DNA binding domain and a C-terminal dimerization domain. Each *B. subtilis* PerR monomer contains a structural metal (Zn^{2+})-binding site in the dimerization domain and a regulatory metal (Fe^{2+} or Mn^{2+})-binding site in the interdomain region. The structural metal is required for proper folding and dimeric assembly, and the regulatory metal allows PerR to interact with DNA motifs (*perR* box) present in the promoter regions of regulated genes (5–8). Upon exposure of *B. subtilis* PerR to H_2O_2 or O_2, two histidine residues that participate in regulatory metal coordination are oxidized, and a global conformational change is triggered (9–11). As a result, PerR dissociates from DNA, and target genes are transcribed by RNA polymerase.

[5] The abbreviations used are: ROS, reactive oxygen species; PerR, peroxide stress regulator; *Bs*PerR, *B. subtilis* PerR; *Li*PerR, *L. interrogans* PerR; Fur, ferric uptake regulator; ICP-MS, inductively coupled plasma mass spectrometry; EMJH, Ellinghausen–McCullough–Johnson–Harris; r.m.s., root mean square; PDB, Protein Data Bank; qRT-PCR, quantitative RT-PCR.

Leptospira are among the few examples of Gram-negative bacteria that possess a PerR-like regulator involved in controlling defenses against peroxide stress (12). These aerobic bacteria of the spirochetal phylum have pathogenic representatives that are the causative agents of leptospirosis, a widespread zoonotic disease (13, 14). Leptospirosis is transmitted to animals and humans by exposure to soils and water contaminated with the urine of reservoir animals carrying pathogenic *Leptospira*. Once having penetrated an organism, *Leptospira* enter the bloodstream and rapidly disseminate to multiple tissues and organs, including kidney, liver, and lungs (15). Clinical manifestations range from a mild flu-like febrile state to more severe and fatal cases leading to hemorrhages and multiple-organ failure (16). Although recognized as an emerging disease and a significant health threat among impoverished populations in developing countries and tropical areas (17), leptospirosis is a neglected and underdiagnosed disease. In addition, the lack of efficient tools and techniques for genetic manipulation of *Leptospira* spp. has greatly hampered our understanding of the mechanism of pathogenicity and virulence as well as the basic biology of this pathogen (13, 14).

Several lines of evidence have indicated the importance of ROS production during infection by *Leptospira*. The internalization of pathogenic *Leptospira* by macrophages and concomitant production of ROS has been demonstrated *in vitro* (18), and leptospirosis-associated oxidative stress has been observed in patients (19) and infected animals (20). Several studies have reported the production of peroxide and other ROS in lung, kidney, and freshly voided urine (21–23), which are colonized by pathogenic *Leptospira*. In addition, catalase is required not only for survival in the presence of H_2O_2 but also for virulence (24), and *perR* is up-regulated when cells are grown in rats (25). These findings strongly suggest a role of PerR in the adaptation of pathogenic *Leptospira* to a mammalian host.

An intriguing particularity of leptospiral PerR, in contrast to most Fur-like regulators, is the absence of a structural metal-binding site. To gain insight into this class of PerR and the molecular mechanism of PerR function in *Leptospira*, we have carried out a functional, biochemical, and structural characterization of this transcriptional regulator. We show that the binding of *Leptospira interrogans* PerR with its promoter region is metal-dependent, and we report the crystal structure of the homodimeric PerR from *L. interrogans*, which provides a snapshot of the metal-induced conformational switch required for DNA binding and dissociation. We have also investigated the effect of *perR* inactivation on the growth of *Leptospira* in conditions similar to those encountered in a mammalian host.

Results

Crystal structure of L. interrogans PerR

Leptospira spp. encode a PerR ORF that shares about 30% amino acid identity with PerRs encoded by other bacteria (*Campylobacter jejuni*, *B. subtilis*, *Staphylococcus aureus*, and *Streptococcus pyogenes*) (Fig. S1*A*). Alignment of the ORF sequence encoded by the pathogen *L. interrogans* serovar Copenhagenii (LIC12034, *Li*PerR) with that of the well-characterized *B. subtilis* (*Bs*PerR) shows a conservation of the five

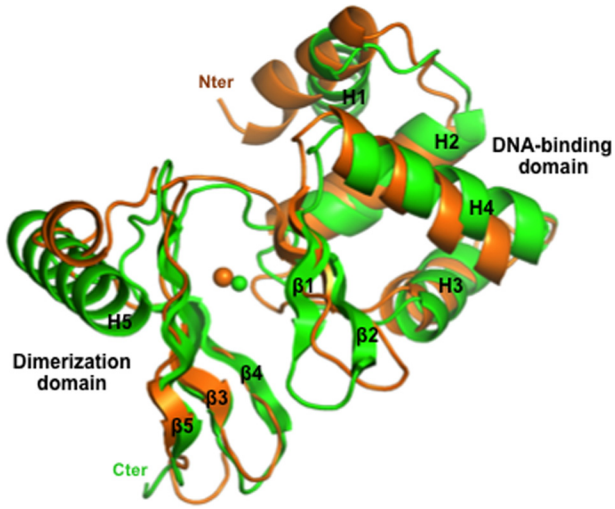

Figure 1. Comparison of the three-dimensional structures of *L. interrogans* and *B. subtilis* PerRs. *Li*PerR monomer A (*green*) is superimposed with the *Bs*PerR-Zn-Mn monomer (PDB entry 3F8N; *orange*), both represented by a *ribbon diagram*. *Green* and *orange spheres* represent *Li*PerR and *Bs*PerR zinc and manganese ions, respectively, in the regulatory metal-binding site. *Nter* and *Cter*, N and C termini, respectively. Secondary structure elements are *labeled*.

residues (His^{37}-Asp^{85}-His^{91}-His^{93}-Asp^{104}, *Bs*PerR primary sequence numbering) that coordinate the regulatory metal (Fig. S1*A*). Surprisingly, the canonical Cys_4 consensus motif that coordinates the structural metal (Cys^{96}, Cys^{99}, Cys^{136}, and Cys^{139}, *Bs*PerR primary sequence numbering) required for PerR dimeric assembly is absent in the primary sequence of *Li*PerR. PerR orthologues in other *Leptospira* strains, including *L. interrogans* serovar Manilae (LManV2_280031), *Leptospira borgpetersenii* serovar Hardjo-Bovis (LBJ_1600), and *Leptospira biflexa* serovar Patoc (LEPBIa2461), also lack the Cys_4 consensus motif (Fig. S1*B*). In contrast, this 4-cysteinate motif is conserved in all PerR regulators whose structures have previously been solved and in most PerR and Fur regulators from sequenced genomes.

To characterize the conformation and assembly of a PerR devoid of a structural metal-binding site, we solved the crystal structure of the *Li*PerR. The protein crystallized as an asymmetric homodimer with two independent monomers (chains A and B) in the asymmetric unit. The electron density could be traced from residue 1 to 145 in both monomers. Each monomer adopts the characteristic two-domain organization of Fur-like regulators with an N-terminal DNA-binding domain and a C-terminal dimerization domain. The N-terminal domain (residues 1–84) contains four α-helices (H1–H4), followed by a two-stranded antiparallel β-sheet (β1, β2) (Fig. 1). Helices H2, H3, and H4 form a trihelical bundle arranged in a helix-turn-helix DNA-binding motif. The putative DNA-binding helix (H4, residues 54–68) is well conserved in other PerRs (Fig. S1). The C-terminal domain (residues 91–145) consists of a long helix (H5, residues 107–127) and three β strands (β3, β4, and β5) which are involved in dimerization of the regulator. The N- and C-terminal domains of each monomer are connected by a flexible hinge region (residues 85–90), which adopts significantly different conformations in monomers A and B (see below). The overall structure of monomer A is similar to that of the *Bs*PerR-Zn-Mn structure (PDB entry 3F8N; Fig. 1) with the

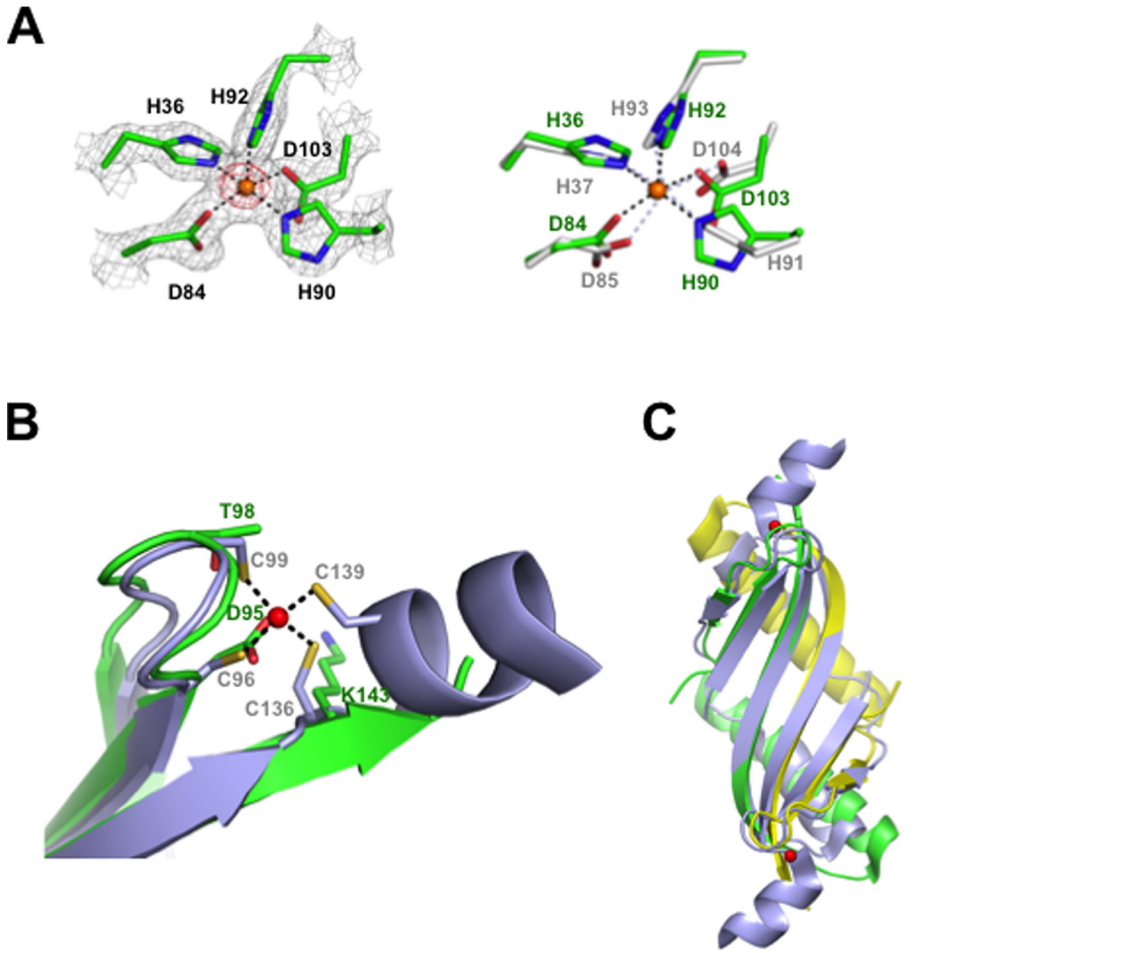

Figure 2. Metal binding in *L. interrogans* PerR. *A*, detailed view of the regulatory binding site of LiPerR (*left*) and LiPerR superimposed with BsPerR (LiPerR in *green* and BsPerR (PDB entry 3F8N) in *white*) (*right*). The coordination residues are labeled in *green* and *gray* for LiPerR and BsPerR, respectively, and the metals in the regulatory metal-binding sites are represented by *orange* (zinc for LiPerR) or *blue* (manganese for BsPerR) *spheres*. Ligand coordination is symbolized by *black* and *blue dashed lines* for LiPerR and BsPerR, respectively. The electron density map (*gray contours*, *left*) was calculated with coefficients $2F_{obs} - F_{calc}$ and is contoured at 2σ. An anomalous difference map (*red contours*, *left*) is shown contoured at 20σ. *B*, detailed view of the structural metal-binding site of *Bs*PerR (PDB entry 2FE3; *blue*) superimposed with the corresponding region in *Li*PerR (chain A; *green*). The cysteine residues coordinating the structural metal in *Bs*PerR (zinc, symbolized by a *red sphere*) are indicated in *blue*, and the superimposed residues in *Li*PerR are shown in *green*. *C*, overall view of the *Bs*PerR dimerization domain (PDB entry 2FE3; *blue*) superimposed with the corresponding region in *Li*PerR (chains A and B in *green* and *yellow*, respectively). The structural zinc coordinated by *Bs*PerR is represented by a *red sphere*.

helix-turn-helix DNA-binding domain (H2-H3-H4-β1-β2, residues 20–84) and the β-sheet of the dimerization domain (β3-β4-β5, residues 91–104 and 129–144) bearing the greatest structural similarities (r.m.s. deviations of 2.16 and 1.54 Å, respectively, for 70 and 30 structurally equivalent Cα atoms).

In *Bs*PerR, the regulatory metal (Fe^{2+} and Mn^{2+}, as determined by *in vivo* studies (5)) is coordinated with square pyramid geometry (His^{37}-Asp^{85}-His^{91}-His^{93}-Asp^{104}, PDB entry 3F8N (6)). In *S. pyogenes*, the metal present in the regulatory metal-binding site (Zn^{2+} or Ni^{2+}) is coordinated with octahedral geometry by six residues (His^{4}-His^{6}-Asn^{15}-His^{19}-His^{97}-His^{99}) (PDB entry 4I7H (26); PDB entry 4LMY (27)). In the *Li*PerR crystal structure, zinc was the only metal present, as determined by X-ray fluorescence measurements. This metal is coordinated by residues His^{36}, Asp^{84}, His^{90}, His^{92}, and Asp^{103}, which are nitrogen/oxygen donors (Fig. 2*A*). The regulatory metal-binding site is arranged as a distorted square pyramid with His^{92} at the apical position and His^{36}, Asp^{84}, His^{90}, and Asp^{103} at the base. These residues can be closely superimposed with the corresponding residues in the *Bs*PerR structure (Fig. 2*A*).

As expected from the amino acid sequence, the crystal structure of *Li*PerR confirmed the absence of the canonical Cys_4 consensus motif involved in the structural metal coordination (Fig. 2*B*). Three of the four canonical Cys_4 residues of *Bs*PerR (Cys^{96}, Cys^{99}, and Cys^{136}) were structurally aligned with Asp^{95}, Thr^{98}, and Lys^{143}, respectively, in *Li*PerR (Fig. 2*B*). This structural alignment differs from the amino acid sequence alignment (Fig. S1). In *Bs*PerR, the structural zinc locks the three β strands (β3, β4, and β5) in close proximity to form a six-stranded β sheet that stabilizes the dimeric assembly (8, 26, 27). *Li*PerR crystallized as a dimer stabilized by helix H5 and a six-stranded β sheet formed by strands β3, β4, and β5 in the C-terminal domains of each monomer (Fig. 2*C*). The total buried surface area in the dimer interface is 3570 $Å^2$. The β strands involved in dimerization of *Li*PerR and *Bs*PerR adopt similar topology and can be closely superimposed (Fig. 2*C*), indicating that the β sheet could be formed, and dimerization occurred in the absence of a structural metal in *Li*PerR. Moreover, analysis of purified PerR by dynamic light scattering indicated that the protein is dimeric in solution (Fig. S2). Therefore, structural

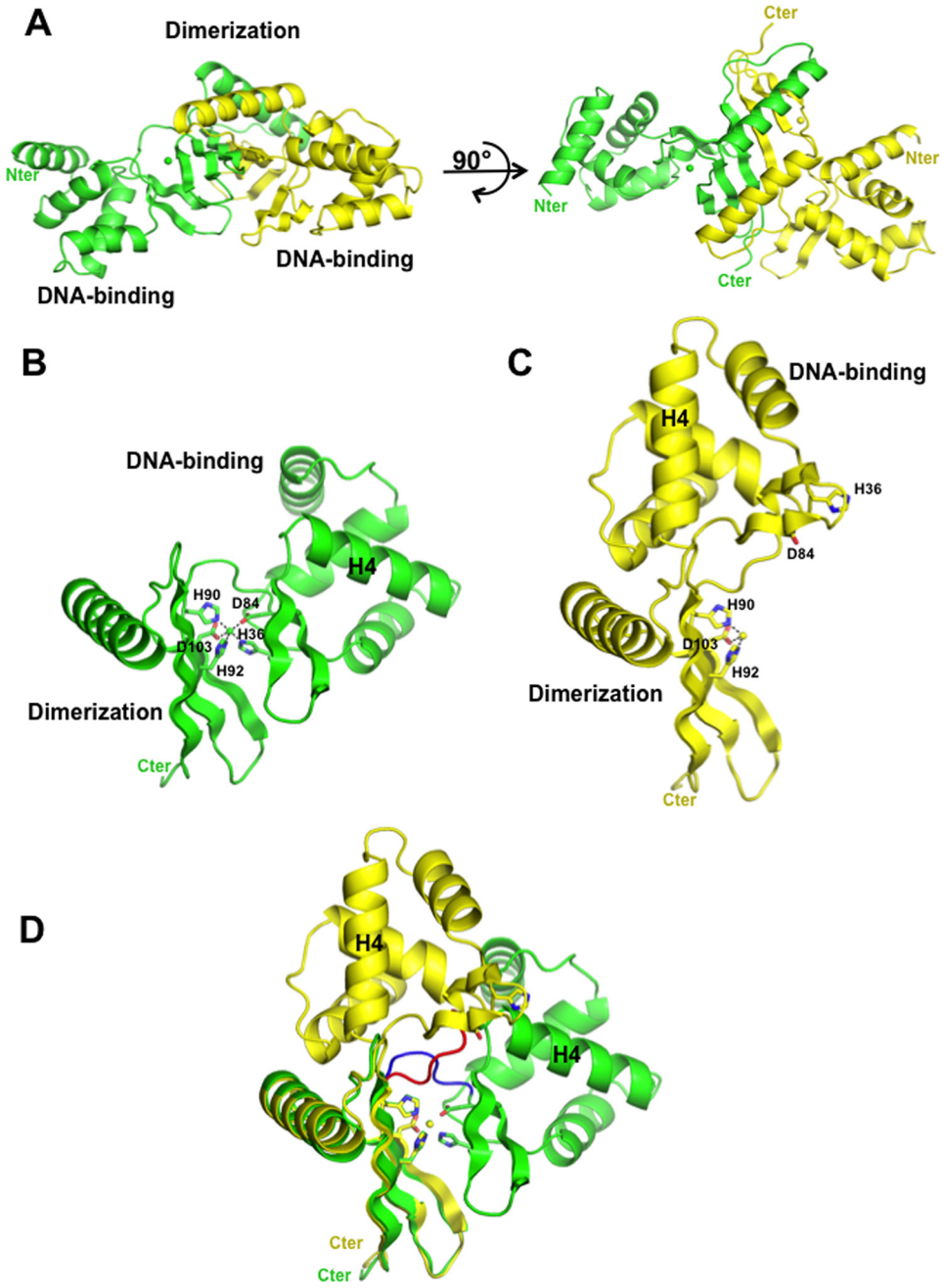

Figure 3. Crystal structure of the *L. interrogans* PerR dimer. *A*, two orthogonal views of the crystallized *Li*PerR dimer are represented with monomer A in *green* and monomer B in *yellow*. Zinc ions bound to monomers A and B are symbolized by *green* and *yellow spheres*, respectively. *B* and *C*, individual monomer A (*B*) and monomer B (*C*) are represented with their respective zinc ion coordination. The H4 helix is *labeled*. *D*, monomers A (*green*) and B (*yellow*) are shown superimposed by their C-terminal dimerization domains. The hinge region (residues 85–89) is *colored blue* and *red* in monomers A and B, respectively.

analysis of *Li*PerR shows that the absence of a structural metal-binding site does not affect the overall topology or oligomerization of the protein.

The asymmetric PerR dimer reveals a conformational switch upon regulatory metal coordination

In the crystallized *Li*PerR dimer, monomers A and B share similar overall folding within the individual N-terminal and C-terminal domains, with r.m.s. deviations for equivalent Cα positions of 0.47 and 0.70 Å, respectively (Fig. 3*A*), but the relative orientation of the two domains differs significantly, resulting in a globally asymmetric overall structure (Fig. 3, *B* and *C*). Superposition of the C-terminal domains of the two monomers shows that the centroid of the N-terminal DNA binding domain of monomer B was shifted by 22 Å from the position in monomer A (Fig. 3*D*). Zinc coordination in the regulatory metal-binding site of monomer A involves five amino acid residues (His^{36}, Asp^{84}, His^{90}, His^{92}, and Asp^{103}) (Figs. 2*A* and 3*B*), whereas zinc coordination in monomer B involves only three residues (His^{90}, His^{92}, and Asp^{103}), which are fully exposed in the C-terminal domain (Fig. 3*C*). His^{36} and Asp^{84}, which participate in the regulatory metal coordination in monomer A, are fully exposed in monomer B with main-chain Cα positions displaced by 22 and 16 Å, respectively (Fig. 3*C*). Consequently, His^{36} and Asp^{84}

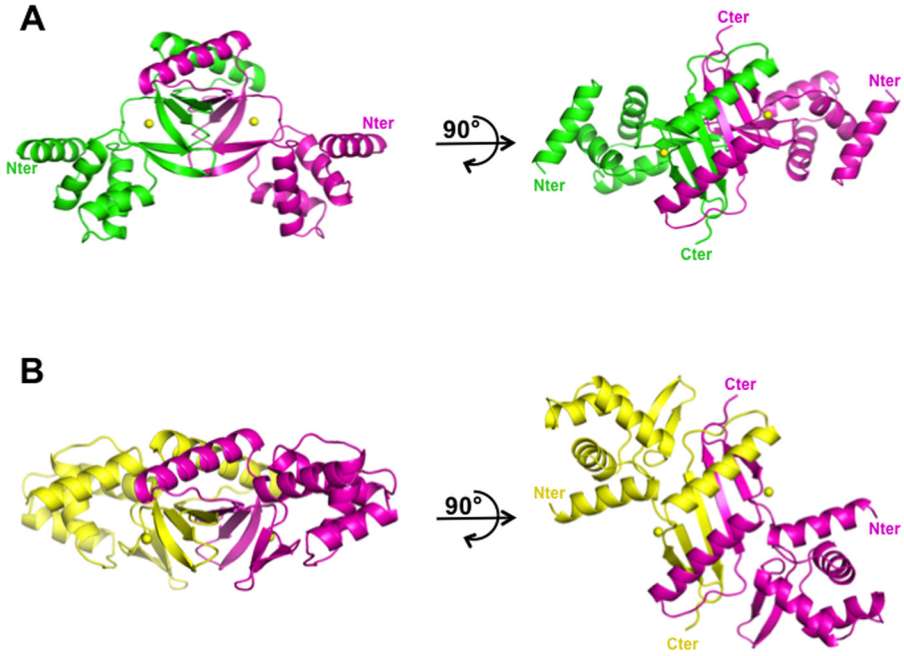

Figure 4. Modeled *L. interrogans* PerR symmetrical dimers. Symmetrical dimers A (*A*) and B (*B*) were generated by superimposing the C-terminal domains of monomers A and B, respectively. *Yellow spheres*, zinc ions.

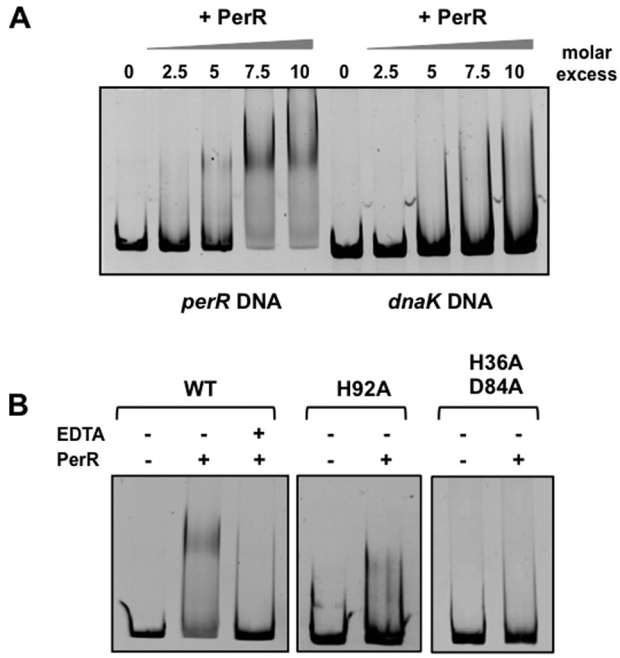

Figure 5. DNA binding by PerR is metal-dependent. *A*, 1 pmol of 429-bp DNA fragments containing the *perR* or *dnaK* promoter regions, respectively, were incubated with 0, 2.5, 5, 7.5, or 10 pmol of purified PerR for 1 h at 37 °C. PerR-DNA binding was analyzed by EMSA as described under "Experimental procedures." Data are representative of three independent experiments. *B*, 1 pmol of the 429-bp DNA fragment containing the *perR* promoter was incubated with 0 or 10 pmol of purified WT PerR or H92A or H36AD84A PerR variants. When indicated, the reaction was performed in the presence of 20 mM EDTA. PerR-DNA complexes were analyzed as described above. Data are representative of three independent experiments.

in monomer B do not participate in zinc coordination, leaving the partial metal-binding site exposed to solvent.

Models of symmetrical dimers of *Li*PerR were generated by superimposing the C-terminal domains of monomers A and B, respectively. The modeled symmetrical dimer of monomer A, with complete regulatory metal coordination in both monomers, exhibits the typical caliper-like structure of Fur family regulators with the regulatory metal bound as in the Mn^{2+}-bound conformation of *Bs*PerR (Fig. 4*A* and Fig. S3). The symmetrical dimer of monomer B, in which the regulatory metal-binding sites are disrupted, has an open planar conformation (Fig. 4*B*) comparable with the apo-conformation of *Bs*PerR (Fig. S3). The orientations of the two DNA-binding helices H4 in symmetrical dimers A and B dramatically differ, and the spacing is significantly greater in symmetrical dimer B. The two helices H4 are 32.6 Å apart in symmetrical dimer A (distance between the Cα atoms of the Lys^{63} in helix H4). The equivalent distance in the Mn^{2+}-bound *Bs*PerR (distance between the Cα atoms of Arg^{64}) is 36 Å, suggesting that the symmetrical dimer A adopts a conformation suitable for DNA binding, whereas the conformation of symmetrical dimer B is incompatible with DNA binding.

LiPerR binds to the perR upstream promoter region in a metal-dependent manner

To investigate the ability of *Li*PerR to bind DNA, recombinant PerR was purified and incubated with a DNA fragment containing the *perR* promoter region. As shown in Fig. 5*A*, a 7.5-fold molar excess of PerR led to a total shift of DNA. However, this shift was not observed when an equivalent DNA fragment containing the *dnaK* promoter region was mixed with an excess of purified *Li*PerR (Fig. 5*A*) or when the assay was performed in the presence of 20 mM EDTA (Fig. 5*B*). These results indicate that *Li*PerR was able to bind its own promoter region in a metal-dependent manner. Preincubation of the purified proteins with Fe^{2+} in aerobic conditions inhibited the interaction of *Li*PerR with DNA, whereas preincubation with other metals (Mn^{2+}, Cu^{2+}, Co^{2+}, Ni^{+}, or Zn^{2+}) did not significantly affect the interaction with DNA (Fig. S4).

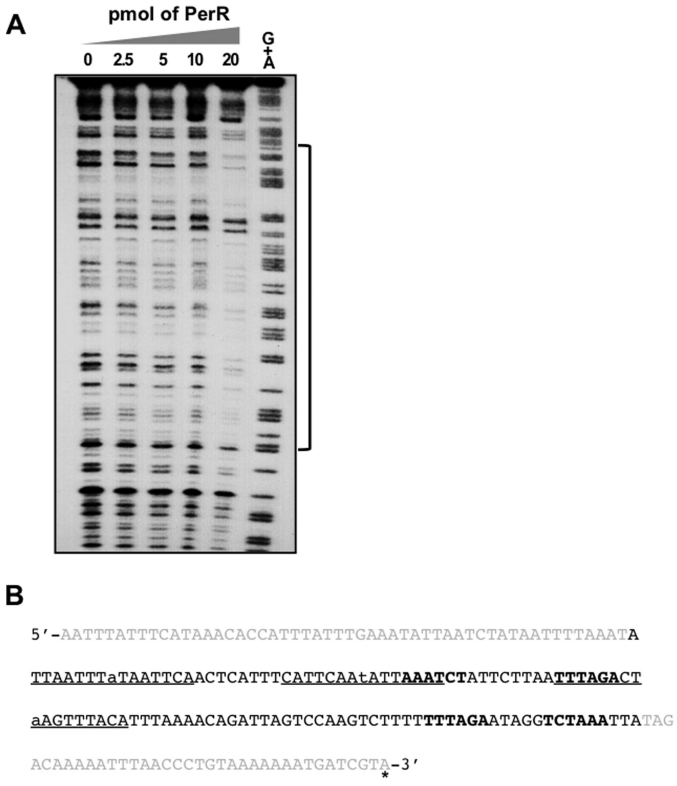

Figure 6. DNA footprint analysis of the *perR* promoter region in *L. interrogans*. *A*, a radiolabeled 200-bp DNA fragment corresponding to the *perR* promoter region (−200 to −1 from the start site of translation) was used as a DNA probe. Various amounts of purified PerR (indicated in pmol of dimer) were incubated with 0.5 pmol of DNA before DNase I digestion. The sequencing ladder by Maxam and Gilbert reaction is shown in the *G+A lane*. A *bracket* indicates the protected region. Data are representative of two independent experiments. *B*, the nucleotide sequence of the DNA fragment used as a probe is shown with the protected sequence in *black*. *Underlined* nucleotides are inverted repeat sequences resembling a *perR* box, and nucleotides in *boldface type* are notable direct repeat motifs. The *asterisk* indicates the transcription site start, which corresponds to the first nucleotide of the ATG translation initiation codon (28).

Analysis of the metal content of the purified recombinant *Li*PerR by inductively coupled plasma mass spectrometry (ICP-MS) (Table S1) showed that the protein contained 0.18 and 0.39 molar eq of Zn^{2+} and Ni^{2+}, respectively, per monomer. Fe^{2+}, Mn^{2+}, and Co^{2+} were present at negligible amounts. These ratios indicate that only a fraction of the PerR subunits contained bound metals. By expressing the recombinant protein in minimal medium and chelating metals after purification (extensive dialysis in the presence of EDTA and use of chelex-treated buffer), it was possible to lower the Ni^{2+} concentration to undetectable levels and the Zn^{2+} concentration to about 0.06 molar eq (Table S1). In this condition, *Li*PerR was still able to bind its promoter region, and this interaction was still inhibited by EDTA, indicating the involvement of a metal (Fig. S5).

To test whether metal coordination was important for DNA binding, we substituted with alanine each of the residues of the regulatory metal-binding site. Single alanine substitutions of His^{36}, Asp^{84}, His^{90}, or Asp^{103} did not affect DNA binding, but when His^{92} was replaced, *Li*PerR did not interact with DNA (Fig. 5*B*), suggesting that this residue plays a central role in maintaining the topology of the regulatory metal-binding site. A double alanine substitution of His^{36} and Asp^{84} also abolished the ability of *Li*PerR to bind DNA (Fig. 5*B*). It is noteworthy that these residues do not participate in regulatory metal binding in monomer B. These findings indicate that the impaired regulatory metal coordination in *Li*PerR is associated with a conformational switch to a non-DNA–binding state.

In *B. subtilis*, derepression of PerR-regulated genes occurs through the oxidation of His^{37} and His^{91} by H_2O_2 or O_2 (9, 11). These residues are highly conserved in PerRs, including *Li*PerR (Fig. S1). When *Li*PerR was incubated with H_2O_2 and subsequently mixed with the promoter region DNA fragment, we did not observe inhibition of DNA binding, but more distinctly resolved shifted bands were observed by EMSA when high H_2O_2 concentrations were used (Fig. S6), indicating that *Li*PerR was still able to bind DNA. Because neither Zn^{2+} nor Ni^{2+} are recognized as regulatory metals that catalyze the H_2O_2-mediated oxidation in previously characterized PerRs, the effects observed when *Li*PerR is pretreated with H_2O_2 are probably not physiologically meaningful.

The association of PerR with DNA was also examined by DNase I footprinting experiments. In the presence of recombinant *Li*PerR purified without metal chelation (*i.e.* containing substoichiometric concentrations of Zn^{2+} and Ni^{2+}), a sequence of 122 bp was protected (Fig. 6*A*). This sequence exhibits three inverted repeat sequences resembling a *perR* box (*underlined* sequences in Fig. 6*B*) as well as four 6-bp motifs (in *boldface type* in Fig. 6*B*). These motifs are located between 38 and 152 nucleotides upstream of the transcription start site of the *perR* ORF, which appears to be identical to the first nucleotide of the translation start codon (28).

Effect of perR inactivation on L. interrogans fitness in host-related conditions

During infection, virulent leptospires are able to survive host conditions, including a temperature of 37 °C, the presence of serum components, and a variety of ROS. To investigate the role of the PerR protein in the pathogen *L. interrogans*, WT and *perR* mutant cells were cultivated in Ellinghausen–McCullough–Johnson–Harris (EMJH) medium in a variety of conditions mimicking those encountered in a mammalian host. It is noteworthy that EMJH medium contains 180 μM Fe^{2+}, the putative physiological regulatory metal of *Li*PerR (29). As shown in Fig. 7*A*, the growth rates of WT and *perR* mutant cells were comparable when cultivated in EMJH medium at 30 °C, the optimal laboratory growth conditions. In the presence of 1 mM H_2O_2, which prevented growth of WT cells, *perR* mutant cells were still able to grow. The increased resistance of the *perR* mutant to H_2O_2 was also assessed by measuring the survival of *Leptospira* cells after a 30-min exposure to 10 mM H_2O_2. In these conditions, WT and *perR* mutant cells had about 0.03 and 100% survival, respectively (Fig. 7*B*). *PerR* was expressed under its native promoter in mutant cells using the pMaORI replicative vector (30), which restored production of PerR, although to lower amounts than observed in WT cells (Fig. 7*C*). Complemented *perR* mutant cells lost their ability to grow and survive in the presence of H_2O_2 (Fig. 7, *C* and *D*). It is interesting to note that *perR* expression increased when *L. interrogans* cells were exposed to sublethal concentrations of H_2O_2 (Fig. 7*E*), indicating that the *perR* promoter had a higher activity in the presence

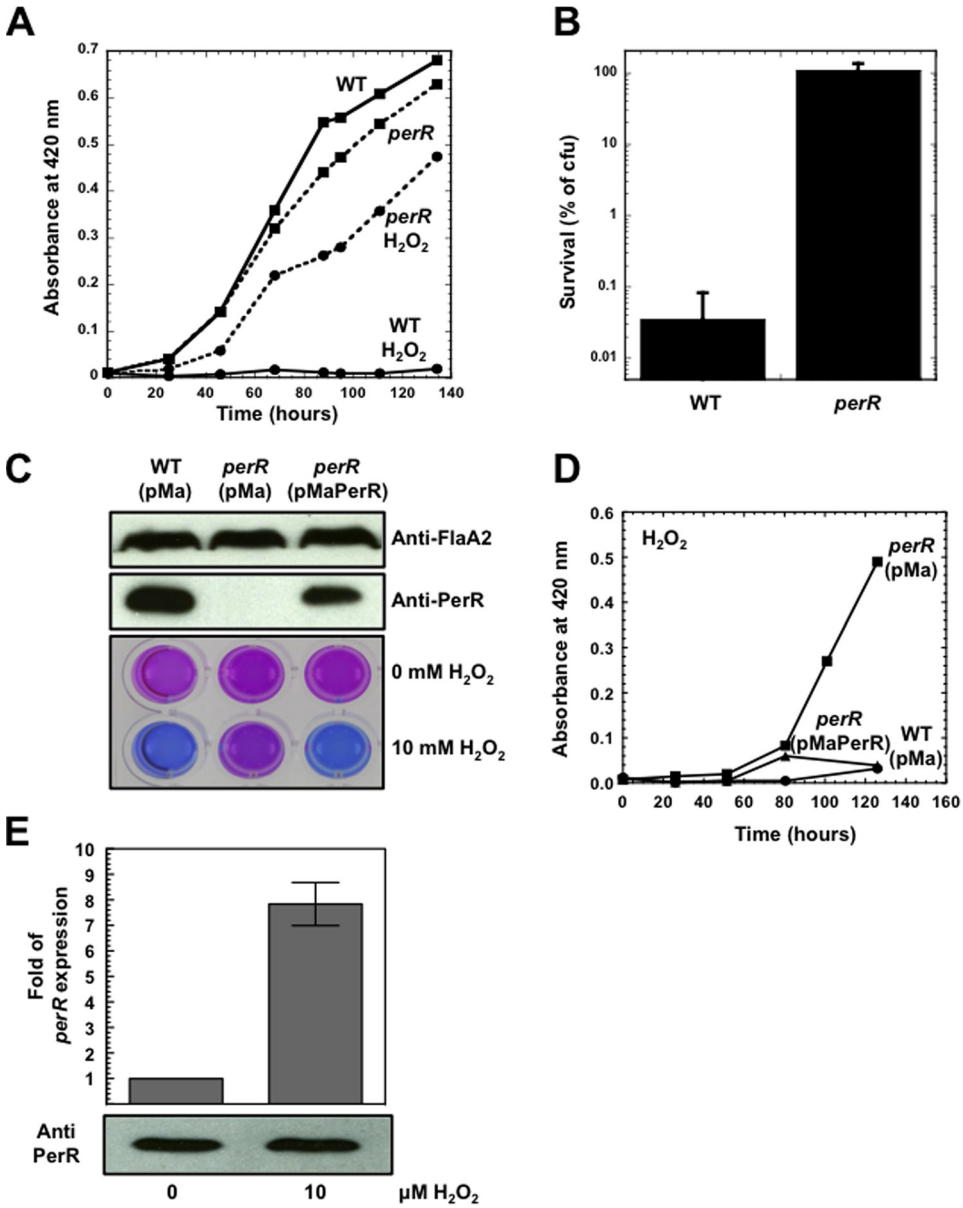

Figure 7. perR expression is stimulated by H_2O_2 and involved in controlling tolerance of *L. interrogans* to peroxide. *A*, WT (*solid lines*) or *perR* mutant (*dashed lines*) cells were cultivated in EMJH medium in the absence (*squares*) or presence (*circles*) of 1 mM H_2O_2 at 30 °C. Cell growth was followed by measuring the absorbance at 420 nm. Data are representative of three independent experiments. *B*, exponentially growing WT or *perR* mutant cells were incubated with 10 mM H_2O_2 for 30 min, and percentage survival was determined as described under "Experimental procedures." Results are shown as the mean and S.D. (*error bars*) of three independent experiments. *C*, 15 μg of total protein extracts from WT and *perR* mutant cells containing the empty pMaORI-expressing vector, WT(pMa) and *perR*(pMa), respectively, and *perR* mutant cells containing the pMaORI vector bearing the *perR* ORF, *perR*(pMaPerR), were loaded on a 15% SDS-polyacrylamide gel and transferred onto nitrocellulose membrane. FlaA2 (equal loading control) and PerR production (*top* and *middle panels*, respectively) were assessed by immunoblot as described under "Experimental procedures." The corresponding cells were incubated for 30 min with 0 or 10 mM H_2O_2, and cell viability was assessed by their capacity to reduce blue resazurin into pink resorufin (*lower panel*). The data are representative of three independent experiments. *D*, WT and *perR* mutant cells containing the empty pMaORI vector, WT(pMa) and *perR*(pMa), respectively, and *perR* mutant cells containing the pMaORI vector bearing the *perR* open reading frame, *perR*(pMaPerR), were cultivated in EMJH medium in the presence of 1 mM H_2O_2 at 30 °C, and cell growth was followed by measuring absorbance at 420 nm. The data are representative of three independent experiments. *E*, *L. interrogans* cells were incubated for 30 min in the presence of 0 or 10 μM H_2O_2 at 30 °C. *PerR* expression was measured by qRT-PCR as described under "Experimental procedures," and PerR cellular content was assessed by immunoblot using 10 μg of total protein extracts as described above. The data are the mean and S.D. of three independent biological repeats (qRT-PCR) or representative of two independent experiments (immunoblot).

of low concentrations of peroxide. However, PerR cellular content did not increase accordingly, as seen by immunoblot (Fig. 7*E*).

We also examined the tolerance of pathogenic *Leptospira* to superoxide stress. WT cells were able to grow in the presence of 2.5 μM paraquat, a superoxide anion-generating reagent, although growth started after an adaptation phase (Fig. 8*A*). In similar conditions, *perR* mutant cells grew more slowly than WT cells. The growth of *perR* mutant cells was also greatly reduced compared with that of WT cells at 37 °C (the host temperature) (Fig. 8*B*) or in the presence of 0.5% human serum (Fig. 8*C*). No effects of *perR* inactivation were observed when cells were cultivated in the presence of 120 mM NaCl (host osmolarity) or in the presence of toxic concentrations of metals

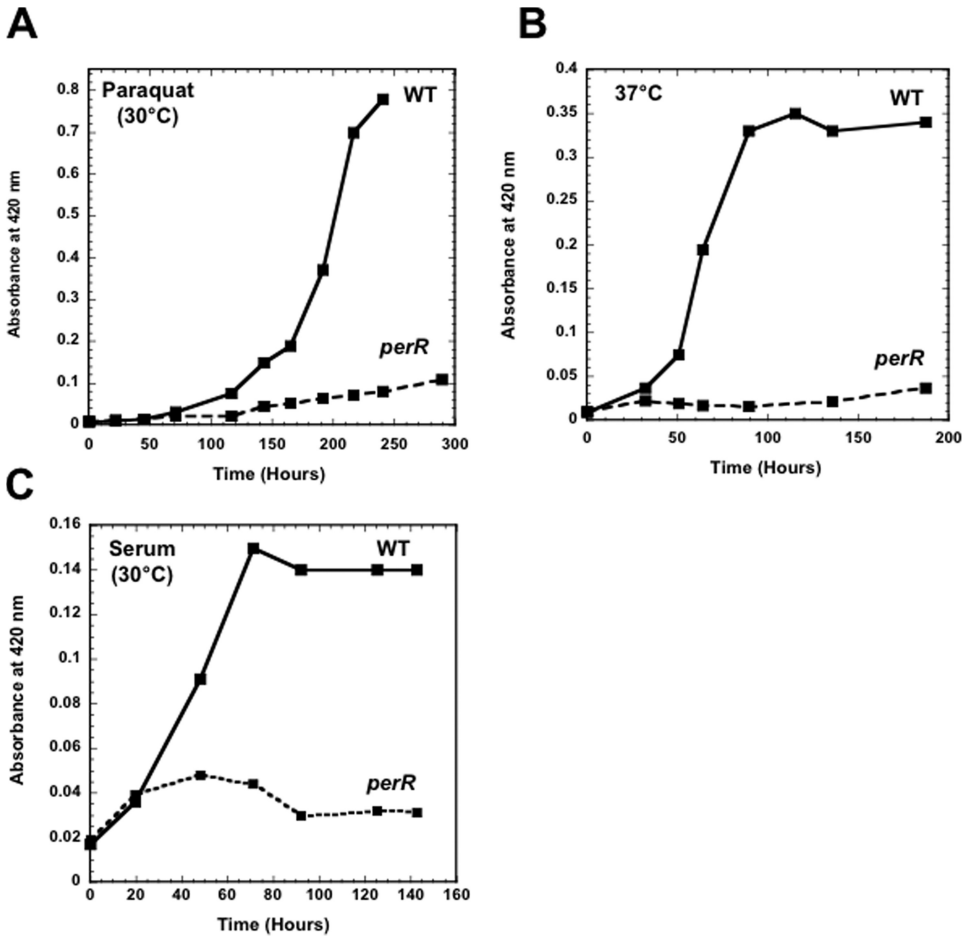

Figure 8. Effect of *perR* inactivation on *L. interrogans* growth in host-related conditions. WT (*solid lines*) or *perR* mutant (*dashed lines*) cells were cultivated in EMJH medium at 30 °C in the presence of 2.5 μM paraquat (*A*), at 37 °C (*B*), or at 30 °C in the presence of 0.5% human serum (*C*). Cell growth was followed as described above. Data are representative of three independent experiments.

(up to 1 mM Cu^{2+}, Co^{2+}, or Zn^{2+}), in the presence of HOCl or with a nitrosative stress–reproducing reagent (diethylamine NONOate) (data not shown). Altogether, these results indicate that the primary role of PerR is to control cell fitness under peroxide stress, although inactivation of *perR* in pathogenic *L. interrogans* also affects growth under other host-related conditions.

Discussion

Extensive biochemical and structural characterizations have been conducted for *Bs*PerR, which has become the paradigm for the PerR family of transcriptional regulators. Until now, crystal structures have been reported for PerRs from only two bacteria, *B. subtilis* and *S. pyogenes* (6, 8, 10, 26, 27). To our knowledge, the crystal structure of the *Li*PerR determined in this study is the first structure of a PerR from a Gram-negative bacterium. The structure shows that the regulatory metal-binding site in *Li*PerR is occupied by zinc, which may have been acquired during protein purification procedures. This zinc ion is coordinated in a manner similar to the regulatory metal (Mn^{2+}) in *Bs*PerR, although zinc is probably not the physiological regulatory metal for *Li*PerR. Indeed, zinc coordination in the regulatory metal-binding site is not unusual and has been observed in other crystal structures of Fur-like regulators (26, 31–33). The wide conservation of the amino acid residues and architecture of the regulatory metal coordination site and the importance of iron in hydroxyl radical production from peroxide argue in favor of iron as the regulatory metal for *Li*PerR. Whether Mn^{2+} could act *in vivo* as a surrogate metal for Fe^{2+} in *Li*PerR remains to be demonstrated. In this study, we show that a *Li*PerR protein preparation containing substoichiometric concentrations of Zn^{2+} interacts with DNA in a metal-dependent manner, but we were not able to determine the exact nature of the metal that supported DNA binding. One hypothesis is that the substoichiometric concentrations of Zn^{2+}, even if not the physiological regulatory metal, are sufficient to promote the DNA binding-prone conformation in a small fraction of the *Li*PerR dimer population. This could explain the presence of smears in the EMSAs indicating a transient or low-affinity interaction with DNA. Alternatively, an additional unidentified metal could be acquired during DNA-binding assays. Our attempts to obtain crystals of *Li*PerR with bound Fe^{2+} in aerobic conditions were unsuccessful, and incubating the purified protein with Mn^{2+} did not increase its ability to bind DNA.

Interestingly, although we could not demonstrate that H_2O_2 inhibits PerR-DNA interaction *in vitro*, we provide experimen-

tal evidence that *perR* expression in *Leptospira* cells is influenced by the cellular H_2O_2 concentration. Because PerR represses its own expression in other bacteria, it is likely that *Li*PerR dissociates from its promoter in the presence of H_2O_2, thereby increasing its expression. Our findings, however, demonstrate that PerR cellular content was not increased accordingly. This suggests another level of regulation by inhibition of translation and/or by protein degradation, as seen for *Bs*PerR (34).

A remarkable feature of the *Li*PerR crystal structure is the globally asymmetric conformation of the homodimer. Monomer A, with complete regulatory metal coordination, has a conformation favorable for DNA binding, whereas monomer B, with disrupted regulatory metal coordination, has an open conformation unfavorable for DNA binding. The two conformations of the *Li*PerR monomers are similar to those observed in the crystal structures of *Bs*PerR in its apo-form (or after oxidation) and upon regulatory metal binding (6, 8, 10). To our knowledge, this study is the first to provide a snapshot of the conformational switch of PerR, showing that this structural change occurs independently in each protomer without disrupting the dimer interface.

It is generally accepted that a structural metal is required to maintain the dimeric assembly of the Fur-like regulators. However, a striking feature of *Li*PerR is the absence of a structural metal-binding site. The wide conservation of the Cys_4 structural metal-binding site in PerRs led to the hypothesis that this site is a distinctive and obligatory feature of PerR regulators (8). Our study demonstrates that *Li*PerR, which is devoid of a structural metal-binding site, is fully functional in regulating peroxide stress *in vivo* and in metal-dependent DNA binding *in vitro* and is susceptible to a metal-driven conformational switch. This study therefore challenges the generality of the role of a structural metal to stabilize PerR dimers. It is interesting to note that the structural metal-binding site is absent in all leptospiral PerRs (pathogens as well as saprophytes) (Fig. S1), although other putative Fur-like regulators in leptospiral species do contain the Cys_4 motif. The Fur regulators from *Pseudomonas aeruginosa* and *Magnetospirillum gryphiswaldense* are two other examples of Fur-like regulators devoid of a structural metal-binding site (32, 35). Phylogenetic studies will be required to understand the conservation and the evolution of this trait.

Increased resistance to H_2O_2 has been associated with *perR* inactivation in *L. interrogans* (12) and in many other bacterial species (36–41). In *L. interrogans*, catalase and cytochrome *c* peroxidase-encoding genes are up-regulated in the absence of PerR, indicating that the protein represses these genes either directly or indirectly (12). We have shown here that a *perR* mutant has a several-log greater percentage survival than WT cells in the presence of H_2O_2 and that *perR* transcript cellular content is enhanced in the presence of H_2O_2. These results confirm the critical role of *L. interrogans* PerR in repressing the defense against hydrogen peroxide and also very likely in sensing H_2O_2.

PerR regulators have been shown to be crucial for the virulence of many bacteria (40, 42–46) partly because regulation of oxidative and peroxide stress is important for the adaptation of pathogenic bacteria to the host environment. However, if the role of PerR regulators were only restricted to repression of peroxide resistance genes, *perR* mutants with greater peroxidase activities would have a survival advantage in the host environment. The PerR regulators may therefore promote the expression of bacterial factors that favor virulence, as observed previously in *S. pyogenes* (47). By studying the fitness of the *perR* mutant in different conditions, we have found that this regulator may help to promote cell growth at the host temperature and in the presence of superoxide anion radicals and human serum. As a pathogen that disseminates through the bloodstream, *Leptospira* will encounter these conditions in the host. Our findings are consistent with a recent study reporting an increase in *perR* expression levels when *Leptospira* were cultivated in the peritoneal cavity of rats (25). Interestingly, about 30 ORFs are deregulated in the *perR* mutant (12), and one-third of these genes are of unknown function. Progress in understanding of the role of *Li*PerR in stress and host adaptation will require improvements of the efficiency of allelic exchange in pathogenic *Leptospira*.

In conclusion, this study shows that *Leptospira* PerR exists in two conformations: an open conformation that does not bind DNA and a caliper-like DNA-binding conformation (Fig. 9). Regulatory metal coordination shifts the equilibrium toward the DNA-binding conformation, and exposure to peroxide very likely leads to DNA dissociation. *Li*PerR probably represses its own expression as it represses expression of peroxidases or of other factors necessary to withstand stress. The absence of PerR would therefore be beneficial for survival under conditions such as peroxide stress, and *Leptospira* cells should maintain the PerR to an appropriate steady-state level by regulated proteolysis to avoid repression of key factors. On the other hand, transcriptional repression or activation of other cellular factors that occurs when active PerR binds to their promoters might be necessary for *Leptospira* fitness under other stress conditions.

By characterizing the function and structure of *Li*PerR, our study sheds light on the peculiarity of this regulator. Further studies of leptospiral PerR should provide new insights into the function of the large family of Fur-like transcriptional regulators.

Experimental procedures

Bacterial strains and growth condition

L. interrogans serovar Manilae WT L495 and the *perR* mutant (M776) strains (12) were grown aerobically at 30 °C in EMJH medium (29) with shaking at 100 rpm. EMJH solid medium was prepared by adding 1% (w/v) noble agar to EMJH liquid medium, and plated cells were incubated at 30 °C for 30 days. When necessary, spectinomycin was added at 50 μg/ml. The *perR* mutant M776 strain carries a transposon insertion at 62 bp into the 438-bp LA1857/LIC12037/LManV2_280031 ORF (12).

Escherichia coli strain BL21(DE3) was cultivated at 30 °C in LB or in minimum medium (M9 salts, 0.4% glucose, 1 mM $MgSO_4$) with shaking at 200 rpm. Kanamycin was added at 30 μg/ml when necessary.

Determination of cell viability

Cell survival was determined by incubating exponentially growing *L. interrogans* cells (~10^8/ml) in EMJH medium in the presence or absence of 10 mM H_2O_2 for 30 min at 30 °C. Cells were then diluted in EMJH medium without H_2O_2 and plated

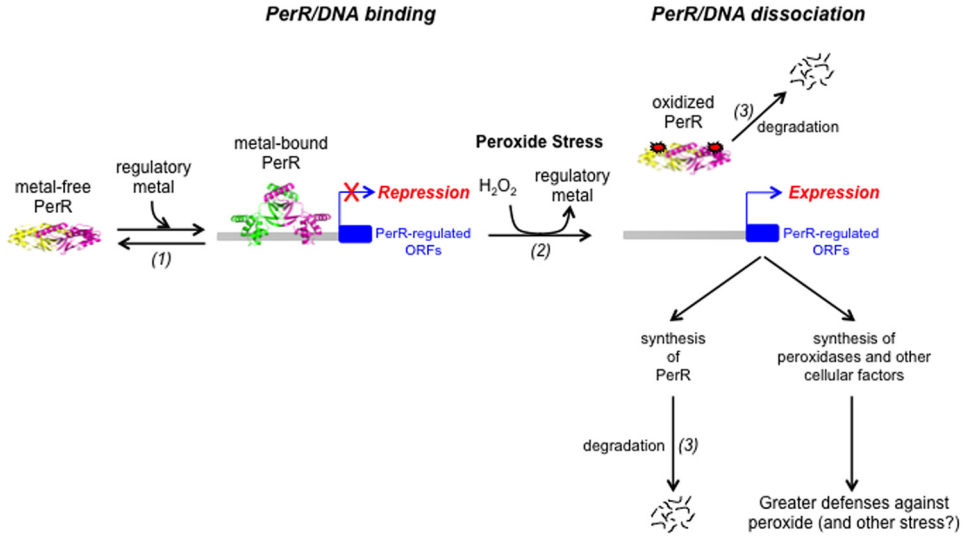

Figure 9. PerR metal-induced allosteric conformational change in *Leptospira* adaptation to stress. Regulatory metal coordination triggers a conformational switch allowing DNA binding (*1*). H_2O_2 oxidation of leptospiral PerR would lead to DNA dissociation (*2*). This would account for the increase in *perR* expression as seen in our study. However, our findings indicate that protein production is not increased accordingly, suggesting another level of regulation, probably by proteolysis (*3*). This additional control would allow *Leptospira* to lower PerR cellular content and prevent repression of peroxidase-encoding genes (or genes encoding other defense activities) during oxidative stress.

on solid EMJH medium. After a 1-month incubation at 30 °C, the colonies were counted, and percentage survival (percentage of cfu) was calculated as the ratio of cfu for cells incubated in the presence of H_2O_2 to that of cells incubated in the absence of H_2O_2. For the colorimetric survival assay, 20 μl of cells were incubated with resazurin (Alamar Blue reagent, Life Technologies, Inc.) for 24 h.

Production and purification of recombinant L. interrogans PerR and its variants

The LIC12034 ORF was amplified from *L. interrogans* serovar Copenhageni strain Fiocruz L1-130 by PCR using the Lic12034-Nhe5 and Lic12034-Hind3 primers (Table S2) and cloned into the pET28b vector (Novagen) between the NheI and HindIII sites. The plasmid obtained (pNB123) allowed the production of an N-terminal His-tagged PerR. PerR variants were obtained by replacing the indicated amino acid residues with alanine using the QuikChange multisite-directed mutagenesis kit (Agilent Technologies) according to the manufacturer's recommendation and with the primers listed in Table S2. All amino acid substitutions were confirmed by DNA sequencing.

E. coli strain BL21(DE3) was transformed with the pNB123 plasmid and grown to exponential phase at 30 °C in LB medium supplemented with kanamycin. Protein expression was then induced with 1 mM isopropyl-β-D-thiogalactopyranoside for 4 h. Cells were harvested by centrifugation and lysed by sonication in buffer A (50 mM NaH_2PO_4, pH 8.0, 300 mM NaCl, 10 mM imidazole, 10% glycerol). The soluble fraction obtained after 1 h of centrifugation at 40,000 × *g* at 4 °C was loaded on nickel-nitrilotriacetic acid resin (Qiagen) equilibrated in buffer A. The resin was washed with buffer A, and His-tagged proteins were eluted with buffer B (50 mM NaH_2PO_4, pH 8.0, 300 mM NaCl, 250 mM imidazole, 10% glycerol). After elution, His-tagged proteins were dialyzed against buffer C (25 mM Tris-HCl, pH 8.0, 100 mM NaCl, 1 mM DTT), and the His_6 tag was then cleaved with biotinylated thrombin (ThermoScientific) for 16 h at 14 °C. Biotinylated thrombin was removed using a streptavidin-agarose resin provided in the Biotinylated Cleavage/Capture kit (Thermo Scientific) according to the manufacturer's recommendations. Traces of uncut His_6PerR were eliminated by subjecting the protein to a nickel-nitrilotriacetic acid column. The flow-through was collected and dialyzed against buffer D (25 mM Tris-HCl, pH 7.5, 150 mM NaCl, 1 mM DTT, 10% glycerol) and concentrated. PerR variant proteins were purified as described above for the WT protein.

For metal chelation, PerR preparation was extensively dialyzed against 50 mM Tris-HCl, pH 7.5, 150 mM NaCl, 100 mM EDTA and subsequently against 50 mM Tris-HCl, pH 7.5, 150 mM NaCl, 10 mM EDTA. The protein preparation was concentrated in Chelex-treated buffer containing 50 mM Tris-HCl, pH 7.5, 150 mM NaCl, 10% glycerol.

For crystallization experiments, PerR was purified from *perR*-expressing BL21(DE3) cells as follows. Cells were lysed by French press in 100 mM Tris-HCl, pH 8.0, and 200 mM NaCl. Soluble extract was obtained by centrifugation at 26,800 × *g* for 1 h. Purification was performed by nickel-immobilized metal affinity chromatography using a HiTrap chelating HP column (GE Healthcare) followed by a size-exclusion chromatographic step using a HiLoad™ 16/60 Superdex 75™ column (GE Healthcare) in 100 mM Tris-HCl, pH 8.0, and 200 mM NaCl. Peak fractions containing PerR were pooled and concentrated up to 22.5 mg/ml with a 5-kDa cut-off Vivaspin concentrator (Sartorius). The concentrated protein, with purity >95% as estimated by Coomassie Blue staining on SDS-PAGE, was stored at −80 °C until use.

Analysis of metal content

Preparations of purified *Li*PerR were incubated with 10% HNO_3 for 15 min at 95 °C and subsequently overnight at room temperature. The reaction was diluted to 3.5% HNO_3, and Zn^{2+}, Mn^{2+}, Fe^{2+}, Co^{2+}, and Ni^{2+} concentrations were determined by ICP-MS. All measurements were recorded in dupli-

cate using 3.5% (v/v) HNO_3 and expressed in μM metal/μM PerR monomer.

DNA-binding assays

For EMSA, 429-bp DNA fragments containing the *perR* (LIC12034) and *dnaK* (LIC10524) promoter regions, respectively (−290 to +120, from translation start), were PCR-amplified from *L. interrogans* serovar Copenhageni strain Fiocruz L1-130 using the primers 12034F/12034R and 10524F/10524R, respectively (Table S2). One pmol of these DNA fragments was incubated for 1 h at 37 °C in the presence or absence of the indicated amount of purified recombinant PerR protein in a 20-ml reaction volume containing 20 mM Tris-HCl, pH 7.5, 50 mM KCl, 2 mM DTT, and 10% glycerol. Samples were then analyzed under nondenaturing 6% polyacrylamide gel electrophoresis in 50 mM Tris, pH 7.5, and 50 mM borate. DNA was detected by ethidium bromide staining.

For DNase I footprinting assay, a DNA fragment corresponding to the promoter region of *perR* (−200 to −1, from translation start; 200 bp) was generated by PCR using the primers 12034F2 and 12034R2 and *Pwo* polymerase (Roche Applied Science) (Table S2). Labeling of the template strand with [γ^{32}-P] ATP (PerkinElmer Life Sciences) was performed as described previously (48). Purified recombinant PerR was used for binding assays to radiolabeled DNA (5×10^4 cpm/reaction) at room temperature in a buffer containing 25 mM NaH_2PO_4, pH 8.0, 50 mM NaCl, 2 mM $MgCl_2$, 1 mM DTT, and 10% glycerol. 0.1 mg/ml poly(dI-dC) (Sigma-Aldrich) was added as competitor DNA to avoid nonspecific binding. DNase I treatment and electrophoresis were performed as described previously (49).

Immunoblotting

L. interrogans serovar Manilae strain L495 cells were cultivated until logarithmic phase and lysed by sonication as described previously (30). Total protein extracts were loaded on a 15% SDS-PAGE and transferred on nitrocellulose membrane. PerR and FlaA2 cellular contents were detected as described (30).

RNA purification and qRT-PCR experiments

Exponentially grown *L. interrogans* serovar Manilae strain L495 cells were incubated in the presence or absence of 10 μM H_2O_2 for 30 min at 30 °C. Harvested cells were resuspended in 1 ml of TRIzol (Ambion) and stored at −80 °C. Nucleic acids were extracted with chloroform and precipitated with isopropyl alcohol. Contaminating genomic DNA was removed by DNase treatment using the RNase-free TURBO DNA-free kit (Ambion) as described by the manufacturer. cDNA synthesis was performed with the cDNA synthesis kit (Bio-Rad) according to the manufacturer's recommendation. Quantitative PCR was conducted with the SsoFast EvaGreen Supermix (Bio-Rad) as described previously (24). *perR* ORF expression was measured with the Lic12034qRTF1 and Lic12034qRTR1 primers using *flab* (LA2017/Lic11890/LManV2_290016) as a reference gene (Table S2).

Table 1
Crystallographic parameters and statistics
Values for the highest-resolution shell are shown in parentheses.

Crystal parameters and data statistics	
Space group	p21
Unit cell dimensions	
a, *b*, *c* (Å)	48.68, 56.10, 68.79
β (degrees)	105.82
V_m (Å^3/Da)	2.66
Resolution (Å)	46.8–1.90 (2.00–1.90)
Unique reflections	27475 (3919)
Multiplicity	6.3 (6.2)
R_{merge}	0.066 (0.852)
R_{pim}	0.043 (0.566)
Completeness (%)	97.3 (95.3)
$\langle I/\sigma(I)\rangle$	13.9 (2.6)
$CC_{½}$	0.997 (0.789)
Refinement	
Resolution (Å)	46.8–1.90 (1.98–1.90)
R value, working set	0.203 (0.327)
R_{free}	0.234 (0.344)
No. of reflections	26716 (2613)
Non-hydrogen atoms	2326
Protein residues	292
Water molecules	173
Zn^{2+} ions	
Monomer A	Occupancy 1.0, *B*-factor 33.1
Monomer B	Occupancy 1.0, *B*-factor 40.7
K^+ ions	1
r.m.s. deviations from ideal	
Bond length (Å)	0.010
Bond angles (degrees)	1.14
Ramachandran plot (%)	
Preferred regions	98.2
Allowed regions	1.40
Outliers (%)	0.4

Crystallization, data collection, structure determination, and refinement

Crystallization screening trials for *Leptospira* PerR were carried out by the sitting drop vapor-diffusion method with a Mosquito® (TTP Labtech) automated nanoliter dispensing system. Sitting drops of 400 nl were set up in Greiner plates for 672 commercially available screening solutions with a 1:1 mixture of protein at 22.7 mg/ml equilibrated against 150 μl of reservoir solution. The plates were stored at 18 °C in a RockImager (Formulatrix) automated imaging system to monitor crystal growth. Best crystals were obtained with a solution of 0.2 M potassium sodium tartrate and 20% (w/v) PEG 3350 (condition D1 from commercial kit PEG/Ion, Hampton Research). Crystals with dimensions of up to 0.1 × 0.1 × 0.2 mm appeared within 2 weeks. For data collection, the crystals were flash-cooled in liquid nitrogen using a paratone-paraffin oil mixture (50%/50%) as cryoprotectant.

X-ray diffraction data were collected on beamline PROXIMA 1 at synchrotron SOLEIL (St. Aubin, France). X-ray fluorescence emission scans revealed the presence of zinc and the absence of iron or other metals in the crystals. The structure was solved by the single-wavelength anomalous dispersion method with data collected just above the zinc K-edge as determined by the X-ray absorption scan (Fig. S7). The diffraction images were integrated with XDS (50). Heavy-atom sites were located with SHELXD (51). Phasing, density modification, and preliminary chain tracing were performed with Phaser (52), Parrot, and Buccaneer from the CCP4 software suite (53). The models were improved by alternate cycles of manual adjustment and model building with Coot (54) and refinement with BUSTER (55, 56). Crystallographic data and refinement statistics are shown in Table 1. All structural figures were generated with PyMOL (57).

Author contributions—M. K., R. T., A. L., B. B., and P. W. performed experiments. F. S., A. H., S. D., M. P., and N. B. conceived, performed, and analyzed experiments. N. B. conceived and coordinated the study and wrote the paper. All authors approved the final version of the manuscript.

Acknowledgments—We acknowledge SOLEIL for provision of synchrotron radiation facilities, and we thank the staff of beamline PROXIMA 1 for assistance. We are grateful to Gerald Murray and Ben Adler for providing the perR mutant. We thank Gouzel Karimova, Isabelle Michaud-Soret, and Victor Duarte for critically reading the manuscript and for helpful discussions.

References

1. Winterbourn, C. C. (2008) Reconciling the chemistry and biology of reactive oxygen species. *Nat. Chem. Biol.* **4,** 278–286 CrossRef Medline
2. Robinson, J. M. (2008) Reactive oxygen species in phagocytic leukocytes. *Histochem. Cell Biol.* **130,** 281–297 CrossRef Medline
3. Dubbs, J. M., and Mongkolsuk, S. (2012) Peroxide-sensing transcriptional regulators in bacteria. *J. Bacteriol.* **194,** 5495–5503 CrossRef Medline
4. Giedroc, D. P. (2009) Hydrogen peroxide sensing in *Bacillus subtilis*: it is all about the (metallo)regulator. *Mol. Microbiol.* **73,** 1–4 CrossRef Medline
5. Fuangthong, M., Herbig, A. F., Bsat, N., and Helmann, J. D. (2002) Regulation of the *Bacillus subtilis* fur and perR genes by PerR: not all members of the PerR regulon are peroxide inducible. *J. Bacteriol.* **184,** 3276–3286 CrossRef Medline
6. Jacquamet, L., Traoré, D. A., Ferrer, J. L., Proux, O., Testemale, D., Hazemann, J. L., Nazarenko, E., El Ghazouani, A., Caux-Thang, C., Duarte, V., and Latour, J. M. (2009) Structural characterization of the active form of PerR: insights into the metal-induced activation of PerR and Fur proteins for DNA binding. *Mol. Microbiol.* **73,** 20–31 CrossRef Medline
7. Lee, J. W., and Helmann, J. D. (2006) Biochemical characterization of the structural Zn^{2+} site in the *Bacillus subtilis* peroxide sensor PerR. *J. Biol. Chem.* **281,** 23567–23578 CrossRef Medline
8. Traore, D. A., El Ghazouani, A., Ilango, S., Dupuy, J., Jacquamet, L., Ferrer, J. L., Caux-Thang, C., Duarte, V., and Latour, J. M. (2006) Crystal structure of the apo-PerR-Zn protein from *Bacillus subtilis*. *Mol. Microbiol.* **61,** 1211–1219 CrossRef Medline
9. Lee, J. W., and Helmann, J. D. (2006) The PerR transcription factor senses H_2O_2 by metal-catalysed histidine oxidation. *Nature* **440,** 363–367 CrossRef Medline
10. Traoré, D. A., El Ghazouani, A., Jacquamet, L., Borel, F., Ferrer, J. L., Lascoux, D., Ravanat, J. L., Jaquinod, M., Blondin, G., Caux-Thang, C., Duarte, V., and Latour, J. M. (2009) Structural and functional characterization of 2-oxo-histidine in oxidized PerR protein. *Nat. Chem. Biol.* **5,** 53–59 CrossRef Medline
11. Sethu, R., Gouré, E., Signor, L., Caux-Thang, C., Clémancey, M., Duarte, V., and Latour, J. M. (2016) Reaction of PerR with molecular oxygen may assist H_2O_2 sensing in anaerobes. *ACS Chem. Biol.* **11,** 1438–1444 CrossRef Medline
12. Lo, M., Murray, G. L., Khoo, C. A., Haake, D. A., Zuerner, R. L., and Adler, B. (2010) Transcriptional response of *Leptospira interrogans* to iron limitation and characterization of a PerR homolog. *Infect. Immun.* **78,** 4850–4859 CrossRef Medline
13. Ko, A. I., Goarant, C., and Picardeau, M. (2009) *Leptospira*: the dawn of the molecular genetics era for an emerging zoonotic pathogen. *Nat. Rev. Microbiol.* **7,** 736–747 CrossRef Medline
14. Picardeau, M. (2017) Virulence of the zoonotic agent of leptospirosis: still terra incognita? *Nat. Rev. Microbiol.* **15,** 297–307 CrossRef Medline
15. Adler, B. (2014) Pathogenesis of leptospirosis: cellular and molecular aspects. *Vet. Microbiol.* **172,** 353–358 CrossRef Medline
16. Haake, D. A., and Levett, P. N. (2015) Leptospirosis in humans. *Curr. Top. Microbiol. Immunol.* **387,** 65–97 Medline
17. Costa, F., Hagan, J. E., Calcagno, J., Kane, M., Torgerson, P., Martinez-Silveira, M. S., Stein, C., Abela-Ridder, B., and Ko, A. I. (2015) Global morbidity and mortality of leptospirosis: a systematic review. *PLoS Negl. Trop. Dis.* **9,** e0003898 CrossRef Medline
18. Marangoni, A., Accardo, S., Aldini, R., Guardigli, M., Cavrini, F., Sambri, V., Montagnani, M., Roda, A., and Cevenini, R. (2006) Production of reactive oxygen species and expression of inducible nitric oxide synthase in rat isolated Kupffer cells stimulated by *Leptospira interrogans* and *Borrelia burgdorferi*. *World J. Gastroenterol.* **12,** 3077–3081 CrossRef Medline
19. Araújo, A. M., Reis, E. A., Athanazio, D. A., Ribeiro, G. S., Hagan, J. E., Araujo, G. C., Damião, A. O., Couto, N. S., Ko, A. I., Noronha-Dutra, A., and Reis, M. G. (2014) Oxidative stress markers correlate with renal dysfunction and thrombocytopenia in severe leptospirosis. *Am J. Trop. Med. Hyg.* **90,** 719–723 CrossRef Medline
20. Erdogan, H. M., Karapehlivan, M., Citil, M., Atakisi, O., Uzlu, E., and Unver, A. (2008) Serum sialic acid and oxidative stress parameters changes in cattle with leptospirosis. *Vet. Res. Commun.* **32,** 333–339 CrossRef Medline
21. Long, L. H., Evans, P. J., and Halliwell, B. (1999) Hydrogen peroxide in human urine: implications for antioxidant defense and redox regulation. *Biochem. Biophys. Res. Commun.* **262,** 605–609 CrossRef Medline
22. Rovin, B. H., Wurst, E., and Kohan, D. E. (1990) Production of reactive oxygen species by tubular epithelial cells in culture. *Kidney Int.* **37,** 1509–1514 CrossRef Medline
23. Shlyonsky, V., Boom, A., and Mies, F. (2016) Hydrogen peroxide and sodium transport in the lung and kidney. *Biomed. Res. Int.* **2016,** 9512807 Medline
24. Eshghi, A., Lourdault, K., Murray, G. L., Bartpho, T., Sermswan, R. W., Picardeau, M., Adler, B., Snarr, B., Zuerner, R. L., and Cameron, C. E. (2012) *Leptospira interrogans* catalase is required for resistance to H_2O_2 and for virulence. *Infect. Immun.* **11,** 3892–3899 CrossRef Medline
25. Caimano, M. J., Sivasankaran, S. K., Allard, A., Hurley, D., Hokamp, K., Grassmann, A. A., Hinton, J. C., and Nally, J. E. (2014) A model system for studying the transcriptomic and physiological changes associated with mammalian host-adaptation by *Leptospira interrogans* serovar Copenhageni. *PLoS Pathog.* **10,** e1004004 CrossRef Medline
26. Makthal, N., Rastegari, S., Sanson, M., Ma, Z., Olsen, R. J., Helmann, J. D., Musser, J. M., and Kumaraswami, M. (2013) Crystal structure of peroxide stress regulator from *Streptococcus pyogenes* provides functional insights into the mechanism of oxidative stress sensing. *J. Biol. Chem.* **288,** 18311–18324 CrossRef Medline
27. Lin, C. S., Chao, S. Y., Hammel, M., Nix, J. C., Tseng, H. L., Tsou, C. C., Fei, C. H., Chiou, H. S., Jeng, U. S., Lin, Y. S., Chuang, W. J., Wu, J. J., and Wang, S. (2014) Distinct structural features of the peroxide response regulator from group A *Streptococcus* drive DNA binding. *PLoS One* **9,** e89027 CrossRef Medline
28. Zhukova, A., Fernandes, L. G., Hugon, P., Pappas, C. J., Sismeiro, O., Coppee, J. Y., Becavin, C., Malabat, C., Eshghi, A., Zhang, J. J., Yang, F. X., and Picardeau, M. (2017) Genome-wide transcriptional start site mapping and sRNA identification in the pathogen *Leptospira interrogans*. *Front. Cell Infect. Microbiol.* **7,** 10 CrossRef Medline
29. Ellinghausen, H. C., Jr., and McCullough, W. G. (1965) Nutrition of *Leptospira pomona* and growth of 13 other serotypes: fractionation of oleic albumin complex and a medium of bovine albumin and polysorbate 80. *Am. J. Vet. Res.* **26,** 45–51 Medline
30. Pappas, C. J., Benaroudj, N., and Picardeau, M. (2015) A replicative plasmid vector allows efficient complementation of pathogenic *Leptospira* strains. *Appl. Environ. Microbiol.* **81,** 3176–3181 CrossRef Medline
31. Dian, C., Vitale, S., Leonard, G. A., Bahlawane, C., Fauquant, C., Leduc, D., Muller, C., de Reuse, H., Michaud-Soret, I., and Terradot, L. (2011) The structure of the *Helicobacter pylori* ferric uptake regulator Fur reveals three functional metal binding sites. *Mol. Microbiol.* **79,** 1260–1275 CrossRef Medline
32. Pohl, E., Haller, J. C., Mijovilovich, A., Meyer-Klaucke, W., Garman, E., and Vasil, M. L. (2003) Architecture of a protein central to iron homeostasis: crystal structure and spectroscopic analysis of the ferric uptake regulator. *Mol. Microbiol.* **47,** 903–915 CrossRef Medline

33. Sheikh, M. A., and Taylor, G. L. (2009) Crystal structure of the *Vibrio cholerae* ferric uptake regulator (Fur) reveals insights into metal co-ordination. *Mol. Microbiol.* **72,** 1208–1220 CrossRef Medline
34. Ahn, B. E., and Baker, T. A. (2016) Oxidization without substrate unfolding triggers proteolysis of the peroxide-sensor, PerR. *Proc. Natl. Acad. Sci. U.S.A.* **113,** E23–E31 CrossRef Medline
35. Deng, Z., Wang, Q., Liu, Z., Zhang, M., Machado, A. C., Chiu, T. P., Feng, C., Zhang, Q., Yu, L., Qi, L., Zheng, J., Wang, X., Huo, X., Qi, X., Li, X., *et al.* (2015) Mechanistic insights into metal ion activation and operator recognition by the ferric uptake regulator. *Nat. Commun.* **6,** 7642 CrossRef Medline
36. Brenot, A., King, K. Y., and Caparon, M. G. (2005) The PerR regulon in peroxide resistance and virulence of *Streptococcus pyogenes*. *Mol. Microbiol.* **55,** 221–234 CrossRef Medline
37. Bsat, N., Herbig, A., Casillas-Martinez, L., Setlow, P., and Helmann, J. D. (1998) *Bacillus subtilis* contains multiple Fur homologues: identification of the iron uptake (Fur) and peroxide regulon (PerR) repressors. *Mol. Microbiol.* **29,** 189–198 CrossRef Medline
38. Fujishima, K., Kawada-Matsuo, M., Oogai, Y., Tokuda, M., Torii, M., and Komatsuzawa, H. (2013) dpr and sod in *Streptococcus mutans* are involved in coexistence with *S. sanguinis*, and PerR is associated with resistance to H_2O_2. *Appl. Environ. Microbiol.* **79,** 1436–1443 CrossRef Medline
39. Hillmann, F., Fischer, R. J., Saint-Prix, F., Girbal, L., and Bahl, H. (2008) PerR acts as a switch for oxygen tolerance in the strict anaerobe *Clostridium acetobutylicum*. *Mol. Microbiol.* **68,** 848–860 CrossRef Medline
40. Horsburgh, M. J., Clements, M. O., Crossley, H., Ingham, E., and Foster, S. J. (2001) PerR controls oxidative stress resistance and iron storage proteins and is required for virulence in *Staphylococcus aureus*. *Infect Immun.* **69,** 3744–3754 CrossRef Medline
41. van Vliet, A. H., Baillon, M. L., Penn, C. W., and Ketley, J. M. (1999) *Campylobacter jejuni* contains two fur homologs: characterization of iron-responsive regulation of peroxide stress defense genes by the PerR repressor. *J. Bacteriol.* **181,** 6371–6376 Medline
42. Gryllos, I., Grifantini, R., Colaprico, A., Cary, M. E., Hakansson, A., Carey, D. W., Suarez-Chavez, M., Kalish, L. A., Mitchell, P. D., White, G. L., and Wessels, M. R. (2008) PerR confers phagocytic killing resistance and allows pharyngeal colonization by group A *Streptococcus*. *PLoS Pathog.* **4,** e1000145 CrossRef Medline
43. Palyada, K., Sun, Y. Q., Flint, A., Butcher, J., Naikare, H., and Stintzi, A. (2009) Characterization of the oxidative stress stimulon and PerR regulon of *Campylobacter jejuni*. *BMC Genomics* **10,** 481 CrossRefMedline
44. Rea, R., Hill, C., and Gahan, C. G. (2005) *Listeria monocytogenes* PerR mutants display a small-colony phenotype, increased sensitivity to hydrogen peroxide, and significantly reduced murine virulence. *Appl. Environ. Microbiol.* **71,** 8314–8322 CrossRef Medline
45. Ricci, S., Janulczyk, R., and Bjorck, L. (2002) The regulator PerR is involved in oxidative stress response and iron homeostasis and is necessary for full virulence of *Streptococcus pyogenes*. *Infect. Immun.* **70,** 4968–4976 CrossRef Medline
46. Zhang, T., Ding, Y., Li, T., Wan, Y., Li, W., Chen, H., and Zhou, R. (2012) A Fur-like protein PerR regulates two oxidative stress response related operons dpr and metQIN in *Streptococcus suis*. *BMC Microbiol.* **12,** 85 CrossRef Medline
47. Wen, Y. T., Tsou, C. C., Kuo, H. T., Wang, J. S., Wu, J. J., and Liao, P. C. (2011) Differential secretomics of *Streptococcus pyogenes* reveals a novel peroxide regulator (PerR)-regulated extracellular virulence factor mitogen factor 3 (MF3). *Mol. Cell Proteomics* **10,** M110.007013 CrossRef Medline
48. Derré, I., Rapoport, G., and Msadek, T. (1999) CtsR, a novel regulator of stress and heat shock response, controls clp and molecular chaperone gene expression in gram-positive bacteria. *Mol. Microbiol.* **31,** 117–131 CrossRef Medline
49. Dubrac, S., and Msadek, T. (2004) Identification of genes controlled by the essential YycG/YycF two-component system of *Staphylococcus aureus*. *J. Bacteriol.* **186,** 1175–1181 Medline
50. Kabsch, W. (2010) XDS. *Acta Crystallogr. D Biol. Crystallogr.* **66,** 125–132 CrossRef Medline
51. Sheldrick, G. M. (2008) A short history of SHELX. *Acta Crystallogr. A* **64,** 112–122 CrossRef Medline
52. McCoy, A. J., Grosse-Kunstleve, R. W., Adams, P. D., Winn, M. D., Storoni, L. C., and Read, R. J. (2007) Phaser crystallographic software. *J. Appl. Crystallogr.* **40,** 658–674 CrossRef Medline
53. Winn, M. D., Ballard, C. C., Cowtan, K. D., Dodson, E. J., Emsley, P., Evans, P. R., Keegan, R. M., Krissinel, E. B., Leslie, A. G., McCoy, A., McNicholas, S. J., Murshudov, G. N., Pannu, N. S., Potterton, E. A., Powell, H. R., *et al.* (2011) Overview of the CCP4 suite and current developments. *Acta Crystallogr. D Biol. Crystallogr.* **67,** 235–242 CrossRef Medline
54. Emsley, P., Lohkamp, B., Scott, W. G., and Cowtan, K. (2010) Features and development of Coot. *Acta Crystallogr D Biol. Crystallogr.* **66,** 486–501 CrossRef Medline
55. Blanc, E., Roversi, P., Vonrhein, C., Flensburg, C., Lea, S. M., and Bricogne, G. (2004) Refinement of severely incomplete structures with maximum likelihood in BUSTER-TNT. *Acta Crystallogr. D Biol. Crystallogr.* **60,** 2210–2221 CrossRef Medline
56. Smart, O. S., Womack, T. O., Flensburg, C., Keller, P., Paciorek, W., Sharff, A., Vonrhein, C., and Bricogne, G. (2012) Exploiting structure similarity in refinement: automated NCS and target-structure restraints in BUSTER. *Acta Crystallogr. D Biol. Crystallogr.* **68,** 368–380 CrossRef Medline
57. DeLano, W. L. (2010) *The PyMOL Molecular Graphics System*, version 1.3r1, Schrödinger, LLC, New York